The Journal of Immunology
RESEARCH ARTICLE | AUGUST 15 2014

Cowpox Virus Protein CPXV012 Eludes CTLs by Blocking ATP Binding to TAP

FREE

Rutger D. Luteijn; ... et. al

J Immunol (2014) 193 (4): 1578–1589.
https://doi.org/10.4049/jimmunol.1400964

Cowpox Virus Protein CPXV012 Eludes CTLs by Blocking ATP Binding to TAP

Rutger D. Luteijn,* Hanneke Hoelen,* Elisabeth Kruse,* Wouter F. van Leeuwen,* Jennine Grootens,* Daniëlle Horst,* Martijn Koorengevel,† Jan W. Drijfhout,‡ Elisabeth Kremmer,§ Klaus Früh,¶ Jacques J. Neefjes,‖ Antoinette Killian,† Robert Jan Lebbink,* Maaike E. Ressing,*,[1] and Emmanuel J. H. J. Wiertz*

CD8$^+$ CTLs detect virus-infected cells through recognition of virus-derived peptides presented at the cell surface by MHC class I molecules. The cowpox virus protein CPXV012 deprives the endoplasmic reticulum (ER) lumen of peptides for loading onto newly synthesized MHC class I molecules by inhibiting the transporter associated with Ag processing (TAP). This evasion strategy allows the virus to avoid detection by the immune system. In this article, we show that CPXV012, a 9-kDa type II transmembrane protein, prevents peptide transport by inhibiting ATP binding to TAP. We identified a segment within the ER-luminal domain of CPXV012 that imposes the block in peptide transport by TAP. Biophysical studies show that this domain has a strong affinity for phospholipids that are also abundant in the ER membrane. We discuss these findings in an evolutionary context and show that a frameshift deletion in the CPXV012 gene in an ancestral cowpox virus created the current form of CPXV012 that is capable of inhibiting TAP. In conclusion, our findings indicate that the ER-luminal domain of CPXV012 inserts into the ER membrane, where it interacts with TAP. CPXV012 presumably induces a conformational arrest that precludes ATP binding to TAP and, thus, activity of TAP, thereby preventing the presentation of viral peptides to CTLs. ***The Journal of Immunology*****, 2014, 193: 1578–1589.**

Nucleated cells express MHC class I (MHC I) molecules at their cell surface to present peptides to CD8$^+$ CTLs. Recognition of virus-derived peptides by CTLs results in the elimination of virus-infected cells, allowing control of virus spread.

The majority of peptides presented by MHC I at the surface of infected cells results from proteasomal degradation of proteins within the cytosol (1). These peptides need to cross the endoplasmic reticulum (ER) membrane for loading onto MHC I in the ER lumen. Translocation of peptides over the ER membrane is mediated by the transporter associated with Ag processing (TAP), a heterodimeric ABC transporter composed of two subunits: TAP1 and TAP2. Each subunit contains a cytosolic nucleotide binding domain (NBD) that facilitates the binding and hydrolysis of ATP to drive peptide translocation over the ER membrane. In addition, the TAP1/TAP2 heterodimer contains a transmembrane (TM) domain composed of 9 TM helices of TAP1 intertwined with 10 TM helices of TAP2 (2, 3). TAP forms the center of the MHC class I peptide-loading complex (PLC) and recruits tapasin, a chaperone that binds newly synthesized, "empty" MHC I to the PLC (4, 5). This arrangement facilitates efficient peptide loading of MHC I. In addition, the chaperones calreticulin and ERp57 further stabilize MHC I in the PLC. Once a peptide is loaded onto the peptide-binding domain of MHC I, the MHC I/peptide complex dissociates from the PLC and travels via the Golgi network to the cell surface, where it displays its content to cytotoxic T cells (6).

Large DNA viruses, such as herpesviruses, adenoviruses, and poxviruses, have acquired gene products that allow for specific interference with MHC I function at various stages during its synthesis, assembly, and transport to the cell surface (7). TAP appears to be an attractive target for these viral immune-evasion strategies, because multiple herpesvirus family members encode specific inhibitors for this transporter. The viral TAP inhibitors show no structural homology and use different strategies to interfere with TAP-mediated peptide transport. ICP47 of HSV-1 and HSV-2 acts as a high-affinity competitor for binding of peptides to the cytosolic peptide-binding domain of TAP (8–10). The human CMV protein US6 alters ATP binding to TAP by diminishing ATP binding to TAP1 and promoting ATP binding to TAP2 (11–13). The UL49.5 proteins of most varicelloviruses restrict conformational alterations of TAP that are necessary to drive peptide transport (14, 15). In addition, UL49.5 of bovine herpesvirus (BHV)-1 and BHV-5 induces degradation of TAP1 and TAP2,

*Department of Medical Microbiology, University Medical Center Utrecht, 3584 CX Utrecht, the Netherlands; †Department of Membrane Biochemistry and Biophysics, Utrecht University, 3584 CH Utrecht, the Netherlands; ‡Department of Immunohematology and Blood Transfusion, Leiden University Medical Center, 2333 ZA Leiden, the Netherlands; §Helmholtz Center Munich, German Research Center for Environmental Health, Institute of Molecular Immunology, 81377 Munich, Germany; ¶Vaccine and Gene Therapy Institute, Oregon Health and Science University, Beaverton, OR 97006; and ‖Department of Cell Biology, The Netherlands Cancer Institute, 1066 CX Amsterdam, the Netherlands

[1]Current address: Department of Molecular Cell Biology, Leiden University Medical Center, Leiden, the Netherlands.

Received for publication April 14, 2014. Accepted for publication June 13, 2014.

This work was supported by Veni Grant 916.10.138 from the Netherlands Organization for Scientific Research and Marie Curie Career Integration Grant PCIG-GA-2011-294196 (both to R.J.L.), Netherlands Scientific Organization Vidi Grant 917.76.330 (to M.E.R.), and a grant from the Dutch Diabetes Research Foundation (to E.J.H.J.W.).

Address correspondence and reprint requests to Prof. Emmanuel J.H.J. Wiertz, Department of Medical Microbiology, University Medical Center Utrecht, P.O. Box 85500, 3508 GA Utrecht, the Netherlands. E-mail address: ewiertz@umcutrecht.nl

Abbreviations used in this article: BHV, bovine herpesvirus; CD, circular dichroism; CPXV, cowpox virus; DOPC, 1,2-dioleoyl-*sn*-glycero-3-phosphocholine; DOPS, 1,2-dioleoyl-*sn*-glycero-3-phospho-L-serine; EHV, equid herpesvirus; ER, endoplasmic reticulum; IRES, internal ribosomal entry site; LUV, large unilaminar vesicle; MES, 2-(*N*-morpholino)ethanesulfonic acid; MHC I, MHC class I; MHC II, MHC class II; MJS, MelJuSo; NBD, nucleotide binding domain; NP-40, Nonidet P-40; PLC, peptide-loading complex; TAP, transporter associated with Ag processing; TfR, transferrin receptor; TM, transmembrane.

whereas UL49.5 of equid herpesvirus (EHV)-1 and EHV-4 interferes with ATP binding to the NBDs of TAP (14). BNLF2a of EBV blocks both peptide and ATP binding to TAP (16). Inhibition of TAP-mediated peptide transport was considered to be unique to herpesviruses until the recent identification of the cowpox virus (CPXV) protein CPXV012 as an effective inhibitor of peptide transport by TAP (17, 18).

CPXVs are members of the *Orthopoxvirus* genus, which comprises several clinically and economically important pathogens, including variola virus (the causative agent of smallpox), camelpox virus, and monkeypox virus. CPXVs have the largest genome of all orthopoxviruses and encode an elaborate arsenal of immune-evasion proteins (19). Two of these proteins, CPXV012 and CPXV203, prevent cytotoxic T cell recognition by interfering with MHC I–mediated Ag presentation. CPXV203 inhibits Ag presentation by retaining MHC I/peptide complexes in the ER (20). CPXV203 acts through a KDEL-related KTEL ER-retention motif encoded in its C-terminal domain (20). Deletion of CPXV203 from CPXV only partially restored MHC I surface expression, suggesting the presence of an additional mechanism that is active in MHC I suppression. Indeed, CPXV012 was identified as the second CPXV protein to interfere with MHC I Ag presentation (17, 18). Deletion of both CPXV012 and CPXV203 fully restored MHC I surface levels. Ex vivo, T cells isolated from CPXV-infected mice produced IFN-γ upon stimulation with CPXVΔ012Δ203-infected cells, in contrast with wild-type CPXV-infected cells (18). Furthermore, in vivo experiments showed that mice infected with the CPXVΔ012Δ203 strain survived, whereas mice infected with the wild-type virus succumbed to virus infection (18).

CPXV012 specifically abrogates TAP-mediated peptide translocation through an unknown mechanism, thereby depriving the ER of peptides (17, 18). In this article, we show that CPXV012 inhibits TAP through its ER-luminal domain by interfering with ATP binding to the cytosolic NBDs of TAP. We define the regions within the CPXV012 ER-luminal domain that are critical for inhibition of TAP function and downregulation of MHC I expression. The ER-luminal domain of CPXV012 adopts an α-helical structure in the presence of phospholipids and displays a strong affinity for ER membranes. The ER-luminal domain of CPXV012 binds to TAP and arrests the TAP complex in a conformational state that is unable to acquire energy (ATP), thereby inhibiting the translocation of peptides into the ER. Additionally, we provide an explanation for the emergence of the functional ER domain of CPXV012 in evolution, via the acquisition of a frameshift mutation in the ancestral protein of CPXV012.

Materials and Methods

Cell lines

The human melanoma cell line MelJuSo (MJS) (21) was maintained in RPMI 1640 medium (Invitrogen), supplemented with 10% FCS (PAA Laboratories), 2 mM L-glutamine, 100 U/ml penicillin, and 100 μg/ml streptomycin (complete medium). HEK293T cells used for lentivirus production were maintained in DMEM complete medium (Invitrogen). The retrovirus packaging cell line φNX-A was maintained in IMDM (Invitrogen) complete medium. MJS cells stably transfected with TAP1-eGFP were obtained from E. Reits (Academic Medical Center, Amsterdam, The Netherlands) (22).

Lentivirus and retrovirus production and transduction

A plasmid encoding codon-optimized CPXV012 from CPXV strain Brighton Red with a FLAG-tag at the N terminus (CPXV012) was used as a template for PCR amplification with the primers 5′-CGGGATCCACCATGGACTACAA-3′ and 5′-GCCTCGAGTCATCAGATGATGC-3′. The resulting PCR product was cloned into the pLZRS retroviral vector. EBV-derived BNLF2a with a C-terminal HA tag (BNLF2a) was cloned into the retroviral vector pLZRS, as described previously (16). Genes were cloned upstream of an internal ribosomal entry site (IRES) to allow coexpression of the truncated nerve growth factor receptor (ΔNGFR) as a marker.

CPXV012 and CPXV012 variants were cloned into the lentiviral vector pLV upstream of IRES and eGFP, as described previously (17).

For the production of replication-deficient recombinant retrovirus, pLZRS vectors were transfected into φNX-A packaging cells. MJS cells were transduced with retrovirus, as described previously (23). Cells were FACS sorted to achieve expression of the gene of interest in all cells. For the production of replication-deficient recombinant lentivirus, the lentiviral vector and third-generation packaging vectors pVSV-G, pMDL, and pRSV were cotransfected into HEK293T cells. Lentivirus-containing supernatants were harvested after 3 d of virus production and used to transduce MJS cells by spin infection at 1000 × g for 2 h at 33°C in the presence of 3.2 mg/ml polybrene.

Cells transduced with retrovirus or lentivirus were sorted by flow cytometry (FACSAria II; BD Biosciences).

CPXV012 variants

CPXV012 deletion and substitution variants were generated and cloned into the pLV-IRES eGFP lentiviral vector. For cloning purposes, a silent mutation resulting in an XhoI restriction site was introduced into CPXV012 using primers 1 and 2 (Table I). The following primers (Table I) were used to generate the CPXV012 deletion and substitution variants: primers 2 and 3 for CPXV012-Δcyt, primers 4 and 5 for CPXV012-ΔER, primers 2 and 6 for CPXV012 soluble, primers 7–10 for TfR-CPXV012, primers 2 and 11 for CPXV012-Ala1, primers 2 and 12 for CPXV012-Ala2, primers 4 and 13 for CPXV012-Ala3, primers 4 and 14 for CPXV012-Ala4, primers 4 and 15 for CPXV012-Ala5, primers 2 and 16 for CPXV012-Ala6, and primers 2 and 17 for CPXV012-Ala7.

To ensure proper ER localization of the CPXV012-soluble variant, we replaced the endogenous signal sequence of CPXV012 with the (cleavable) human CD8 signal sequence (24), because CPXV012 is a type II protein with the TM domain acting as a signal sequence. The chimeric protein transferrin receptor (TfR)-CPXV012 was constructed, in which the ER-luminal domain of CPXV012 was fused to amino acid residues 58–88 of the type II TfR. This region in TfR includes part of the cytosolic tail (aa 58–67) and the TM domain (aa 68–88) (25). The two cysteine residues flanking the TfR TM domain were replaced by alanine residues to remove a potential localization and dimerization signal (25). All variants were produced from a bicistronic transcript, encoding CPXV012 followed by an IRES and eGFP.

Ab generation

The CPXV012-specific rat IgG2a mAb 2A8 was generated by immunizing Lou/C rats with OVA-coupled peptide encompassing CPXV012 aa 28–44 (sequence: CSMEHGYFQEGISRFKI).

Abs

The following primary and directly conjugated Abs were used: mouse anti-HLA class I HC HC10 mAb, PE-conjugated mouse anti–HLA-A/B/C W6/32 mAb (AbD Serotec; #MCA81PE), PE-conjugated mouse anti–HLA-DR mouse G46-6 mAb (BD Pharmingen; #347401), mouse anti-calnexin AF8 mAb (kindly provided by M. Brenner, Harvard Medical School, Boston, MA), mouse anti-FLAG M2 mAb (Sigma-Aldrich; #F1804), rabbit anti-tapasin gp48-C (provided by P. Cresswell, Yale School of Medicine, New Haven, CT), rat anti-tapasin 7F6 mAb (provided by R. Tampé, Johann Wolfgang Goethe University, Frankfurt/Main, Germany), mouse anti-TAP1 148.3 mAb (provided by R. Tampé), mouse anti-TAP2 435.4 mAb (provided by P. van Endert, Hospital Necker, Paris, France), rat anti-CPXV012 2A8 mAb, rat anti-GFP RQ2 mAb (MBL; #D153-3), mouse anti-GFP 1E4 mAb (Enzo; #ADI-SAB-500), mouse anti-CD71 (TfR) H68.4 (Invitrogen; #1368xx), and biotin-conjugated mouse anti-NGFR mAb (BD; #557195).

The following secondary Abs were used: HRP-conjugated rabbit anti-rat IgG (DAKO, #P0450), HRP-conjugated goat anti-rat IgG L-chain specific (Jackson ImmunoResearch, #112-035-175), HRP conjugated goat anti-mouse IgG L-chain specific (Jackson ImmunoResearch, #115-035-174), HRP-conjugated goat anti-mouse IgG (Bio-Rad; #172-1011), and allophycocyanin-conjugated streptavidin (BD Pharmingen; #554067).

Coimmunoprecipitation and immunoblotting

Cells were lysed in 0.5% Nonidet P-40 (NP-40) buffer (0.5% NP-40, 50 mM Tris-HCl [pH 7.5], and 5 mM $MgCl_2$) or 1% digitonin buffer (1% digitonin, 50 mM Tris-HCl [pH 7.5], 5 mM $MgCl_2$, and 150 mM NaCl) in the presence of 10 μM leupeptin and 1 mM 4-(2-aminoethyl) benzenesulfonyl fluoride. To remove nuclear fractions, cell lysates were centrifuged at

Table I. Primers used for the generation of CPXV012 deletion and substitution variants

Primer No.	Sequence (5′–3′)
1	ACCGCGGCCACCATGGACTACAAGGACGACGACGACAAGTTCATCATGCGGGAGAGCATCTACAGAGTGATGATCGTG ATCCTGTACCTGAGCCTGATCTCGAGCTTCCTGGTCATCTGCAG
2	AGTGAGCGCTGTCTAGAGGATC
3	ACCGCGGCCACCATGGACTACAAGGACGACGACGACAAGAGAGTGATGATCGTGATCCTGTAC
4	ACCGTCAGATCGCCTGG
5	ATCTAGAGGATCCCCGGGTCATCAGAAGTAGCCGTGTTCCATGC
6	ACCGCGGCCACCATGGCCTTACCAGTGACCGCCTTGCTCCTGCCGCTGGCCTTGCTGCTCCACGCCGCCAGGCCGGAC TACAAGGACGACGACGACAAGCAGGAAGGCATCAGCCGG
7	CCGCGGCCACCATGGACTACAAGGACGACGACGACAAGCCAAAAAGGGCAAGTGGAAGTATCGCCTATGGGACTATTG CTGTGATCG
8	CTTGAACCGGCTGATGCCTTCCTGATAGCCCAAGTAGCCAATCATAAATCCAATCAAGAAAAA, GACGATCACAGCAATAGTCCCATGGC
9	GGAAGGCATCAGCCGGTTCAAGATCTGCCCCTACCACTGGTACAAGCAGCACATGAGCCTGCTGTTCCGGCGGTACTA CCACAAGC
10	AGTGAGCGCTGTCTAGAGGATCCCCGGGTCATCAGATGATGCTGTCCAGCTTGTGGTAGTACCGCCGGAAC
11	ACTCGAGCTTCCTGGTCATCTGCAGCATGGAACACGGCTACTTCGCCGCTGCAGCTGCCCGGTTCAAGATCTGCCCCT AC
12	ACTCGAGCTTCCTGGTCATCTGCAGCATGGAACACGGCTACTTCCAGGAAGGCATCAGCGCCGCTGCAGCTGCCCCCT ACCACTGGTACAAGC
13	TTCTAGAGGATCCCCGGGTCATCAGATGATGCTGTCCAGCTTGTGGTAGTACCGCCGGAACAGCAGGCTCATGTGCTG CTTGGCAGCTGCAGCGGCGCAGATCTTGAACCGGCTGA
14	TTCTAGAGGATCCCCGGGTCATCAGATGATGCTGTCCAGCTTGTGGTAGTACCGCCGGAACAGCAGGGCAGCTGCAGC GGCGTACCAGTGGTAGGGGCAG
15	TTCTAGAGGATCCCCGGGTCATCAGATGATGCTGTCCAGCTTGTGGTAGTAGGCAGCTGCAGCGGCGCTCATGTGCTG CTTGTACC
16	TTCTAGAGGATCCCCGGGTCATCAGATGATGCTGTCGGCAGCTGCAGCGGCCCGCCGGAACAGCAGGC
17	TTCTAGAGGATCCCCGGGTCATCAAGCTGCAGCGGCCAGCTTGTGGTAGTACCGC

12,000 × *g* at 4°C for 20 min. For coimmunoprecipitation experiments, postnuclear digitonin lysates were incubated with protein G-Sepharose beads (GE Healthcare) and the Abs indicated. After overnight incubation at 4°C, samples were washed four times in 0.5% digitonin buffer, and bound fractions were resuspended in TE buffer (20 mM Tris [pH 6.8] and 1 mM EDTA).

To prepare samples for SDS-PAGE separation, coimmunoprecipitation samples and NP-40 postnuclear lysates were boiled in Laemmli sample buffer at 95°C for 5 min. After SDS-PAGE, proteins were transferred to polyvinylidene difluoride membranes (GE Healthcare) and incubated with Abs specific for the indicated proteins, followed by HRP-coupled secondary Abs. Bound Abs were visualized by incubating polyvinylidene difluoride membranes with ECL (Thermo Scientific Pierce) and exposure to Amersham Hyperfilm (GE Healthcare).

Flow cytometry

MHC I and MHC class II (MHC II) cell surface expression was measured by flow cytometry. All washing and Ab-incubation steps were performed in PBS, supplemented with 0.5% BSA and 0.02% sodium azide. For MHC I cell surface expression, cells were incubated with PE-conjugated W6/32 mAb. For MHC II cell surface expression, cells were incubated with PE-conjugated G46-6 Ab. Cells were fixed using 1% formaldehyde in PBS supplemented with 0.5% BSA and 0.02% sodium azide, and flow cytometric parameters were recorded using a FACSCanto II (BD Biosciences). Analysis of flow cytometry data was performed using FlowJo software (TreeStar).

Peptides

Synthetic peptides were prepared by normal Fmoc chemistry using preloaded Tentagel resins, using PyBop/*N*-methylmorpholine for in situ activation and 20% piperidine in *N*-methylpyrrolidinon for Fmoc removal (26). Couplings were performed for 75 min. After final Fmoc removal, peptides were cleaved with trifluoroacetic acid/H_2O 19:1 containing additional scavengers when C or W residues were present in the peptide sequence. Peptides were isolated by ether/pentane precipitation. Peptides were checked for purity using reversed-phase HPLC–mass spectrometry and for integrity using MALDI-TOF mass spectrometry, showing the calculated molecular masses.

Labeling of peptides used for the peptide-transport assay was performed with 5-(iodoacetamide) fluorescein (Fluka Chemie) at pH 7.5 (Na-phosphate in water/acetonitrile 1:1 v/v). The labeled peptides were desalted over Sephadex G-10 and further purified by C18 reversed-phase HPLC. The molecular mass of the labeled peptides was checked using MALDI-TOF mass spectrometry. All other peptides were synthesized with an N-terminal biotin moiety and a C-terminal amide. Cysteines were replaced by the isosteric α-amino-*n*-butyric acid.

Peptide-transport assay

The peptide-transport assay was performed as described (27). Control MJS cells or MJS cells expressing CPXV012 wild-type or CPXV012 variants were permeabilized with streptolysin O (Murex Diagnostics) and incubated with the fluorescein-coupled peptide CVNKTERAY (*N*-linked glycosylation site underlined) in the presence or absence of 10 mM ATP at 37°C for 10 min. Cells were subsequently lysed in Triton X-100 buffer (1% Triton X-100, 500 mM NaCl, 2 mM $MgCl_2$, 50 mM Tris-HCl [pH 8]) and centrifuged at 12,000 × *g* at 4°C for 20 min to remove nuclei and debris. To evaluate peptide transport into the ER, postnuclear lysates were incubated with ConA–Sepharose beads (GE Healthcare), and glycosylated peptides were isolated from the lysate. After washing the beads with the first-wash buffer (0.1% Triton X-100, 500 mM NaCl, 2 mM $MgCl_2$, 50 mM Tris-HCl [pH 8]) and with the second-wash buffer (500 mM NaCl, 50 mM Tris-HCl [pH 8]), peptides were eluted from beads using elution buffer (500 mM mannopyranoside, 10 mM EDTA, 50 mM Tris-HCl [pH 8]), and fluorescent peptides were detected using a FLUOstar Omega (BMG LABTECH) fluorescence plate reader.

ATP-binding assay

The ATP-binding assay was performed as described previously (16). Briefly, control MJS cells or MJS cells expressing BNLF2a or CPXV012 were lysed in 1% digitonin lysis buffer, as described for coimmunoprecipitation and immunoblotting experiments. Cell lysates were centrifuged at 12,000 × g at 4°C for 20 min to remove nuclei. Postnuclear lysates were incubated with hydrated C-8 ATP-agarose beads (13 μM final concentration; Sigma-Aldrich) at 4°C for 2 h. Unbound supernatant was collected, and ATP-bound proteins were eluted from the beads with 500 mM EDTA (ATP-bound fraction). The ATP-bound fraction and unbound supernatant were analyzed for protein content by immunoblotting with the Abs indicated.

Peptide-binding assay

Peptide binding was evaluated as described previously (16). MJS cells stably transfected with TAP1-eGFP and transduced with control retrovirus or retroviruses expressing BNLF2a or CPXV012 were homogenized using a cell cracker (European Molecular Biology Laboratory; chamber 8.020 mm, ball 8.006 mm) to obtain TAP-containing microsomes. These microsomes were incubated with the ^{125}I-labeled peptide 5PS2 (ERYDKSE-[BPA]-L)

containing a photoactivatable bisphenol A cross-linker (28). After incubation on ice for 15 min, the microsomes were washed with PBS, and peptide was covalently linked to binding partners by UV exposure for 10 min on ice using a UVP device (Blak-Ray B-100A) with a mercury lamp (PAR38; Sylvania). Microsomes were lysed in 0.5% CHAPS buffer (0.5% CHAPS, 100 mM Tris-HCl [pH 8], 5 mM $MgCl_2$), and TAP1-eGFP was isolated using the anti-GFP RQ2 mAb and Protein G beads. Samples were separated by SDS-PAGE, as described above, and ^{125}I-labeled peptide binding was visualized by phosphoimaging. A fraction of the unlabeled microsomes was used for immunoblotting with the anti-GFP 1E4 primary Ab and HRP-conjugated anti-mouse IgG secondary Ab.

Preparation of large unilaminar vesicles and circular dichroism

Preparation of large unilaminar vesicles (LUVs) and circular dichroism (CD) spectrum recording were performed as described previously (29). LUVs composed of a mixture of 1,2-dioleoyl-*sn*-glycero-3-phosphocholine (DOPC) and 1,2-dioleoyl-*sn*-glycero-3-phospho-L-serine (DOPS) (Avanti Polar Lipids) in a 7:3 molar ratio were prepared from 5-mM stock solutions of DOPC and DOPS in chloroform in a glass tube. The solvent was evaporated with nitrogen gas, and the resulting lipid film was kept in a vacuum desiccator for 20 min. Lipid films were hydrated in 10 mM 2-(*N*-morpholino)ethanesulfonic acid (MES) buffer (pH 6.2) at a lipid concentration of 5 mM for 30 min. The lipid suspensions were freeze-thawed for 20 cycles at temperatures of approximately −196 and 40°C and subsequently extruded 20 times through 0.2-μm pore size filters (Anotop 10; Whatman, Maidstone, U.K.). A total of 625 μM LUVs and/or 20 μM peptides diluted in 10 mM MES buffer (pH 6.2) were used for measurements. CD spectra were recorded on a Jasco 810 spectropolarimeter (Jasco, Easton, MD) over a wavelength range of 200–250 nm. Measurements were recorded every 1 nm at a scan rate of 20 nm/min at room temperature in cuvettes with a path length of 1.0 mm. Each reported spectrum is the average of five independent scans.

Langmuir monolayer

Peptide-induced changes in the surface pressure of a monomolecular layer (monolayer) of phospholipids at a constant surface area were measured using the Wilhelmy plate method (29). A Teflon trough was filled with 5.0 ml PBS (pH 7.4). The buffer below the monolayer (subphase) was continuously stirred during the measurements. Lipid monolayers were spread from a 1-mM stock solution in chloroform at the air–buffer interface to give an initial surface pressure of 35 mN/m, before 25 μl of a 55-μM freshly prepared stock solution of peptide in DMSO was injected into the subphase, resulting in a final peptide concentration of 0.3 μM.

Results

CPXV012 interacts with an intact MHC class I PLC

CPXV protein CPXV012 impairs MHC I surface expression by inhibiting TAP-mediated peptide transport (17, 18). However, the molecular mechanism that underlies this TAP inhibition is unknown. To study the biochemical and functional characteristics of CPXV012, the viral protein was equipped with an N-terminal FLAG tag and expressed in the human melanoma cell line MJS using lentiviral transduction. As expected, TAP-mediated transport was inhibited in cells expressing FLAG-CPXV012 (Fig. 1A, *upper panel*). Furthermore, expression of FLAG-CPXV012 reduced MHC I surface expression, whereas MHC class II expression remained unaffected (Fig. 1A, *lower panels*), indicating that the FLAG-tagged CPXV012 is functional and selective for MHC I in MJS cells.

To test whether CPXV012 influences the composition of the PLC, individual PLC constituents were isolated from cells lysed in the presence of digitonin to preserve the interactions within the PLC (Fig. 1B). CPXV012 was found to interact with the complex and did not seem to disturb the overall integrity of the PLC, because similar amounts of TAP1, TAP2, and tapasin were coisolated in the presence and absence of CPXV012 (Fig. 1B, compare *lanes 1* and *2* and lanes *5* and *6*). In the presence of CPXV012, the PLC was enriched for MHC I (compare *lanes 1* and *2* and lanes *5*

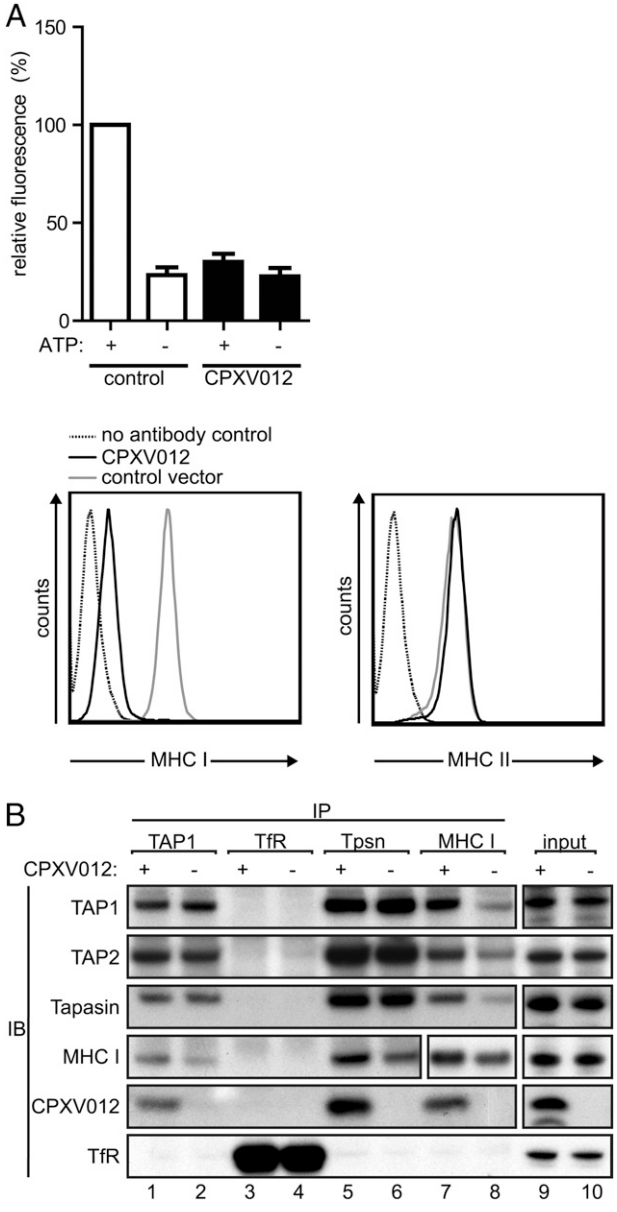

FIGURE 1. CPXV012 interacts with an intact PLC. (**A**) TAP-mediated peptide transport is affected by CPXV012 (*upper panel*). Transport of a fluorescently labeled peptide was measured in MJS cells expressing control vector or CPXV012. To distinguish between active transport and passive diffusion, transport was measured in the presence and absence of ATP. Active transport in cells expressing CPXV012 was compared with transport in control cells expressing eGFP vector only, which was set at 100%. Mean ± SEM from three independent experiments is shown. CPXV012 specifically decreases MHC I surface expression (*lower panels*). Flow cytometric analysis of MHC I and MHC II surface expression on the human melanoma cell line MJS stably expressing CPXV012 (black line) or control vector (gray line). The W6/32 mAb was used for detection of MHC I, and the HLA-DR–specific G46-6 mAb was used for the detection of MHC II. Flow cytometry results are representative of at least three independent experiments. (**B**) CPXV012 interacts with the PLC. TAP1 (mAb 148.3), TfR (mAb H68.4), tapasin (Tpsn; mAb gp48-C), or MHC I (mAb HC10) were immunoprecipitated from digitonin lysates of MJS cells expressing CPXV012 (+ lanes) or control vector (- lanes). Immunoprecipitated proteins were immunoblotted for TAP1 (mAb 148.3), TAP2 (mAb 435.4), tapasin (mAb 7F6), MHC I (mAb HC10), CPXV012 (mAb 2A8), and TfR (mAb H68.4). *Lanes 9* and *10* show input levels of indicated proteins prior to immunoprecipitation. A shorter exposure time was used for *lanes 7* and *8* of the immunoblot for MHC I, as well as for *lanes 9* and *10* of the immunoblots for TAP1, tapasin, MHC I, and CPXV012. Immunoblots are representative of three independent experiments.

and *6*). In agreement with this, more TAP1, TAP2, and tapasin coimmunoprecipitated with MHC I in CPXV012-expressing cells compared with control cells (compare *lanes 7* and *8*). This suggests that peptide loading of MHC I is obstructed by CPXV012, thus delaying the release of MHC I from the PLC.

The interactions between CPXV012 and the components of the PLC were specific, because TfR, an unrelated TM protein, and MHC II (data not shown) were not coisolated. Conversely, isolation of TfR did not yield any PLC proteins (Fig. 1B, *lanes 3* and *4*).

In conclusion, CPXV012 interacts with the PLC in the ER. CPXV012 does not affect the organization of the core components of the PLC (TAP1, TAP2, and tapasin); MHC I appears to accumulate in the PLC, likely as the result of diminished peptide supply.

CPXV012 interferes with ATP binding to TAP

Peptide translocation by TAP can be blocked by viral TAP inhibitors at different stages during the peptide-translocation cycle (30). This cycle initiates with the binding of peptide to the cytosolic peptide-binding domain of TAP, which allows subsequent ATP binding to the cytosolic NBDs (31). ATP binding and hydrolysis at the NBDs cause conformational rearrangements within the transporter that facilitate translocation of the peptides over the ER membrane (31).

We investigated whether CPXV012 affects peptide binding to TAP. An ^{125}I-labeled peptide linked to a photoactivatable cross-linker was incubated with microsomes derived from MJS TAP1-eGFP cells. The cells expressed CPXV012 or the EBV-derived TAP inhibitor BNLF2a, which was previously shown to inhibit peptide binding to TAP (16). After UV cross-linking, TAP1-eGFP was isolated from cell lysates, and ^{125}I-labeled peptide/protein complexes were visualized using phosphoimaging.

In cells expressing CPXV012, radiolabeled peptides were cross-linked to TAP1-eGFP (Fig. 2A, *lane 1*), indicating that CPXV012 does not prevent peptide binding to TAP. As previously reported, ^{125}I-labeled peptides were not cross-linked to TAP1-eGFP in cells expressing BNLF2a (Fig. 2A, *lane 2*), but they were able to cross-link to TAP1-eGFP in control cells (Fig. 2A, *lane 3*) (16).

The next step in the peptide-translocation cycle, ATP binding to TAP, was investigated using an ATP-binding assay (Fig. 2B). Agarose beads coated with immobilized ATP were incubated with digitonin lysates of control cells, cells expressing CPXV012, or cells expressing the TAP inhibitor BNLF2a (16). In addition to peptide binding, BNLF2a reduces ATP binding to TAP (16). Pull-down of ATP-agarose beads yields an ATP-bound fraction and an ATP-unbound supernatant fraction. In control cells, the ATP-bound fraction contained TAP1, TAP2, and tapasin (Fig. 2B, *lane 1*). In contrast, in the ATP-bound fractions of cells expressing CPXV012 or BNLF2a, the amounts of these PLC proteins were reduced (Fig. 2B, compare *lanes 2* and *3* with *lane 1*), whereas these PLC components were abundantly present in the unbound supernatant of CPXV012- and BNLF2a-expressing cells (Fig. 2B, *lanes 5* and *6*). These results suggest that CPXV012 inhibits the TAP transport cycle by interfering with ATP binding to TAP.

The ER-luminal domain of CPXV012 is required for inhibition of TAP

CPXV012 is a type II TM protein consisting of a cytosolic domain, a TM domain, and an ER-luminal domain (Fig. 3A) (17). To establish the contribution of these domains to TAP inhibition, CPXV012 variants were generated lacking the cytosolic domain (CPXV012-Δcyt), the ER-luminal domain (CPXV012-ΔER), or the cytosolic and TM domains (i.e., consisting of only the ER-luminal domain [CPXV012-soluble)] (Fig. 3A). To test the functionality of the CPXV012 variants, their effect on MHC I surface

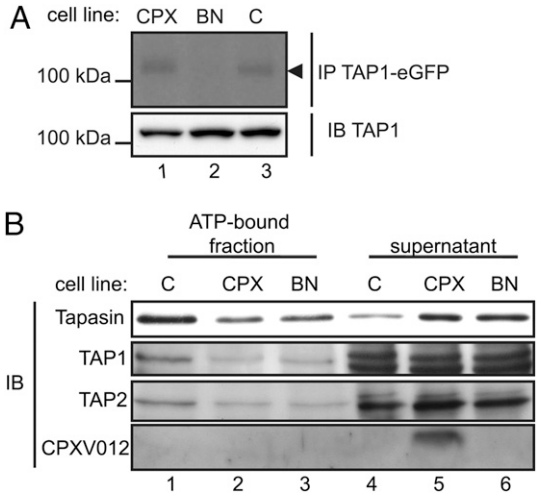

FIGURE 2. CPXV012 interferes with ATP binding to TAP. (**A**) Peptide binding to TAP is not affected by CPXV012. Microsomes were prepared from MJS TAP1-eGFP cells expressing CPXV012 (CPX), EBV protein BNLF2a (BN), or control vector (C) or were incubated with ^{125}I-labeled peptide containing a photoactivatable cross-linker. After UV-induced cross-linking, microsomes were lysed, and TAP1-eGFP was immunoprecipitated with a GFP-specific Ab (mAb 1E4). Immunoprecipitated proteins were separated by SDS-PAGE, and peptide-bound proteins were visualized by phosphoimaging. Arrowhead indicates TAP1-eGFP, which has the expected molecular mass. TAP1-eGFP levels in total lysates of microsomes were determined by immunoblotting (mAb 148.3). A representative of at least three independent experiments is shown. (**B**) ATP binding to TAP is affected by CPXV012. Digitonin lysates of MJS cells expressing control vector (C), CPXV012 (CPX), or BNLF2a (BN) were incubated with ATP-agarose beads. ATP-bound fractions and unbound supernatant were immunoblotted using Abs specific for TAP1 (mAb 148.3), TAP2 (mAb 435.4), tapasin (mAb 7F6), and CPXV012 (mAb 2A8). Immunoblots are representative of at least three independent experiments.

expression was assessed by flow cytometry (Fig. 3B, 3C). As expected, MHC I surface expression was reduced on cells expressing wild-type CPXV012 compared with control cells. MHC I surface levels also were decreased on cells expressing CPXV012 lacking its cytosolic tail (CPXV012-Δcyt), although not as efficiently as for wild-type CPXV012. MHC I surface levels were not reduced on cells expressing CPXV012 lacking its ER-luminal domain (CPXV012-ΔER). This suggests that the ER-luminal region of CPXV012 is essential for MHC I downregulation. In line with this, expression of the C-terminal 34 aa of CPXV012 alone (CPXV012-soluble) reduced MHC I surface expression, albeit less efficiently when compared with wild-type CPXV012. The contribution of the TM domain and cytosolic tail of CPXV012 was investigated further by fusing the ER-luminal domain of CPXV012 to amino acid residues 58–88 of TfR. This region encompasses the TM domain of TfR and a cytosolic stretch of similar length as the cytosolic tail of CPXV012. The resulting TfR-CPXV012 chimera reduced MHC I surface expression as effectively as did wild-type CPXV012. These results indicate that the ER-luminal domain of CPXV012 is sufficient for TAP inhibition; the presence of a cytosolic tail and TM domain improves the efficiency of TAP inhibition, possibly by stabilizing the C-terminal domain of CPXV012 and/or localizing it to the ER membrane.

Protein levels of the CPXV012 variants were assessed by immunoblot analysis (Fig. 3D). Compared with wild-type CPXV012, CPXV012-Δcyt and CPXV012-ΔER were expressed at very low levels (Fig. 3D, *lanes 3* and *4*), whereas CPXV012-soluble was undetectable (Fig. 3D, *lane 5*). In view of the high eGFP levels observed for the CPXV012-soluble IRES eGFP construct, the low protein

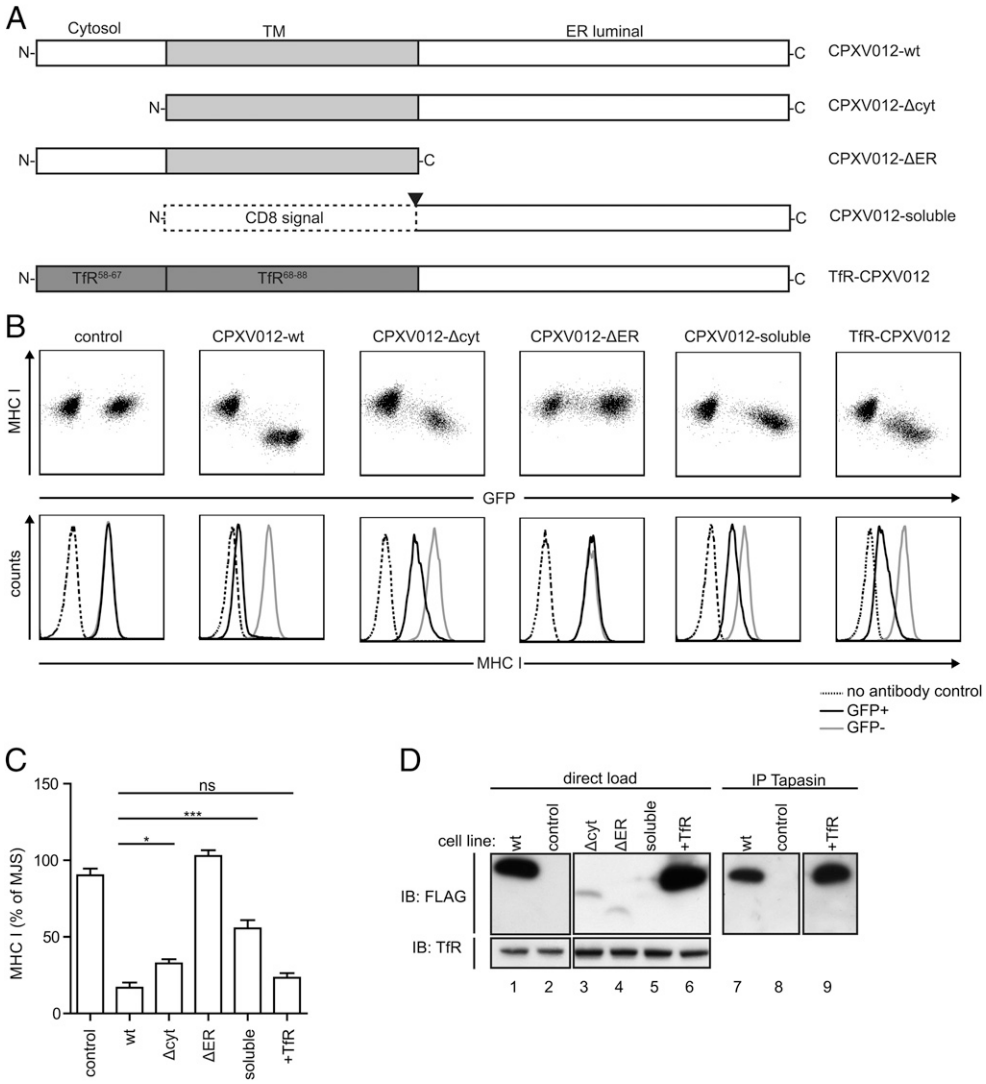

FIGURE 3. The ER-luminal domain of CPXV012 is required for MHC I downregulation. (**A**) Schematic overview of the CPXV012 truncation and substitution variants. The cytosolic, TM, and ER-luminal domains are indicated. Arrowhead indicates the cleavage site of the CD8 signal sequence. (**B**) CPXV012 truncation and substitution variants differentially impact MHC I surface expression. Flow cytometric analysis of MJS cells expressing control vector, wild-type (wt) CPXV012, or the indicated CPXV012 truncation and substitution variants. eGFP expression serves as a marker for the presence of the indicated constructs. $eGFP^+$ cells were mixed with untransduced MJS cells ($eGFP^-$) and stained for MHC I surface levels using W6/32 mAb. (**C**) Mean fluorescence intensity of control vector or CPXV012-expressing cells was compared with $eGFP^-$ MJS cells, set at 100%. Mean ± SEM from three independent experiments is shown. (**D**) Truncation and substitution of CPXV012 domains affect protein stability and binding to the PLC. Digitonin lysates of MJS cells expressing control vector, wild-type CPXV012, or the indicated CPXV012 truncation and substitution variants were separated by SDS-PAGE (*lanes 1–6*). *Lanes 7–9*, Protein complexes isolated using a tapasin-specific Ab (mAb gp46-C) from digitonin lysates were separated by SDS-PAGE. Immunoblotting using Abs specific for FLAG (mAb M2) show expression levels of the indicated CPXV012 variants (*upper panel*). TfR (mAb H68.4) was included as loading control (*lower panel*). Immunoblots are representative of three independent experiments. $***p < 0.001$, $*p < 0.05$, *t* test. C, C terminus; N, N terminus, ns, not significant.

expression is likely caused at a posttranscriptional level. The chimeric TfR-CPXV012 was expressed at levels comparable to those observed for wild-type CPXV012 (Fig. 3D, *lane 6*). Apparently, very low levels of CPXV012 variants are sufficient for downregulating MHC I, as long as the ER-luminal domain of the viral protein is present.

Next, we evaluated the interaction of the ER-luminal domain of CPXV012 with the PLC in the presence of an irrelevant cytosolic tail and TM domain. Abs directed against tapasin were used to isolate the PLC. The amount of chimeric TfR-CPXV012 detected in association with the PLC was comparable to that of wild-type CPXV012 (Fig. 3D, compare *lanes 7* and *9*). Thus, the ER-luminal domain of CPXV012 is sufficient for interaction with the PLC.

The combined results show that the ER-luminal domain of CPXV012 binds to TAP and is sufficient to reduce MHC I surface levels.

Amino acids residues 41–65 of CPXV012 are essential for TAP inhibition

To further delineate the amino acid residues within the ER-luminal domain of CPXV012 involved in inhibiting TAP activity, small stretches of amino acids of FLAG-tagged CPXV012 were substituted with alanine residues (Fig. 4A). To evaluate whether the CPXV012 variants were functional, the MHC I surface levels of CPXV012-expressing cells were compared with those of control MJS cells, expressing eGFP only (Fig. 4B). CPXV012-Ala1 and CPXV012-Ala7 significantly downregulated MHC I surface expression, like wild-type CPXV012 (Fig. 4B). CPXV012-Ala2, CPXV012-Ala3, and CPXV012-Ala6 failed to reduce MHC I expression, whereas CPXV012-Ala4 and CPXV012-Ala5, if anything, increased MHC I surface expression.

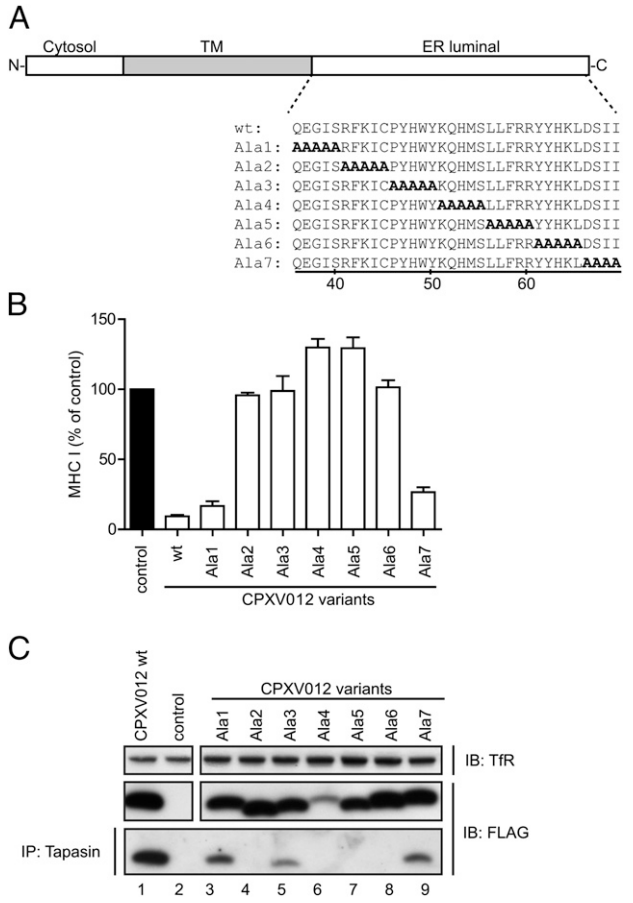

FIGURE 4. Amino acids residues 41–65 of CPXV012 are essential for TAP inhibition. (**A**) Schematic overview of CPXV012 substitution variants. Amino acid residues substituted for alanine are indicated in bold. The amino acid residue position is shown below. (**B**) MHC I surface levels are differentially affected by CPXV012 variants. MHC I surface levels of MJS cells expressing control vector, wild-type (wt) CPXV012, or alanine-substitution variants were analyzed by flow cytometry. Mean fluorescence intensity of CPXV012-expressing cells was compared with cells expressing control vector, set at 100%. Mean ± SEM from three independent experiments is shown. (**C**) CPXV012 variants bind differentially to the PLC. Expression levels of FLAG-tagged CPXV012 variants in total lysates of MJS cells were analyzed by immunoblotting using an anti-FLAG Ab (mAb M2; *middle panel*). The presence of FLAG-CPXV012 variants in the PLC was analyzed by immunoprecipitation of tapasin (mAb gp46-C), followed by immunoblotting using an anti-FLAG Ab (mAb M2; *lower panel*). Anti-TfR Ab (mAb H68.4) was included as loading control (*upper panel*). Immunoblots are representative of three independent experiments.

The expression levels of the CPXV012 variants were examined by immunoblot analysis of cell lysates using an anti-FLAG Ab (Fig. 4C). The protein levels of the variants were similar with the exception of CPXV012-Ala4 (Fig. 4C, *lane 6*), for which expression was lower. CPXV012-Ala4 may be synthesized at a lower rate and/or may be more sensitive to degradation.

Next, we examined the capacity of the CPXV012 variants to associate with the PLC. Cells were lysed in digitonin-containing buffer, and tapasin-specific Abs were used to isolate the PLC. After separation of the proteins by SDS-PAGE, FLAG-specific mAb was used to detect the CPXV012 variants. The variants that were able to abrogate MHC I surface expression also were coisolated with the PLC (CPXV012-Ala1 and CPXV012-Ala7), albeit to a lesser extent than wild-type CPXV012 (Fig. 4C, compare *lanes 1*, *3*, and *9*). Variants that failed to downregulate MHC I also were not isolated from the PLC, with the exception of CPXV012-Ala3 (Fig. 4C, *lane 5*).

These results show that amino acid residues 41–65 of CPXV012 are essential for inhibition of TAP. The failure of CPXV012-Ala3 to inhibit TAP indicates that binding to the PLC alone is not sufficient for MHC I downregulation.

Membrane interaction of the active domain of CPXV012

The ER-luminal domain of CPXV012 is crucial for inhibition of peptide transport by TAP. To assess the structural properties of this domain, we synthesized a peptide corresponding to amino acid residues 36–69 of CPXV012 (CPXV012$^{36–69}$) and investigated the secondary structure of this peptide by CD spectroscopy (Fig. 5A). The far UV CD spectrum of CPXV012$^{36–69}$ obtained in aqueous MES buffer suggested that the peptide adopts a random coil secondary structure. A higher structural order may be induced by lipid membranes, because >30% of the amino acid residues in CPXV012$^{36–69}$ are hydrophobic. Therefore, the CD spectrum of CPXV012$^{36–69}$ was measured in the presence of lipid vesicles consisting of phosphatidylcholine (DOPC) and

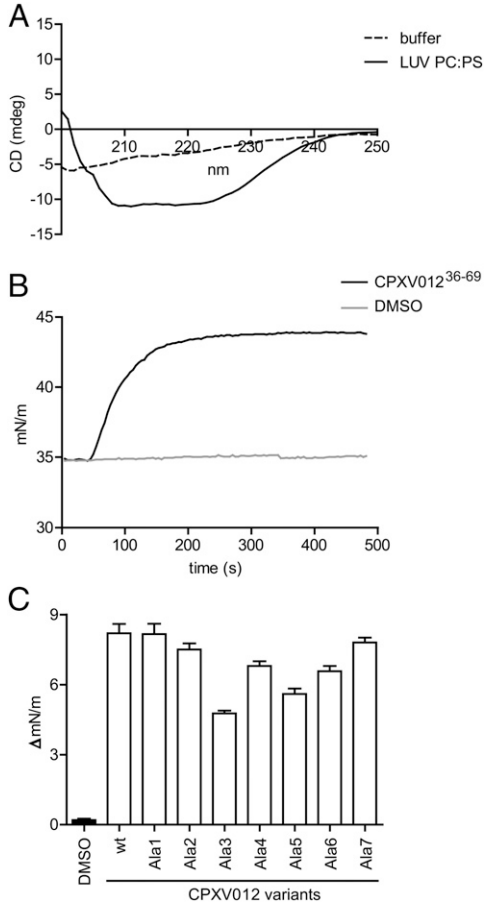

FIGURE 5. Membrane interaction of the active domain of CPXV012. (**A**) CPXV012$^{36–69}$ forms an α-helical secondary structure in the presence of LUVs composed of DOPC and DOPS (7:3). CD spectrum of the ER-luminal domain of CPXV012 was determined in an aqueous buffer or in the presence of LUVs. Results are representative of three independent experiments. (**B**) CPXV012 inserts into lipid monolayers of DOPC and DOPS. Surface pressure profile was measured after injecting CPXV012$^{36–69}$ or DMSO into the lipid monolayer subphase at t = 0 min. Surface pressure was determined using Langmuir monolayers. Results are representative of three independent experiments. (**C**) Surface pressure increase induced by injecting CPXV012$^{36–69}$ and alanine-substitution variants into the lipid monolayer subphase. The amino acid sequence of the peptides corresponds to the ER-luminal domain of the alanine-substitution variants (Ala1–7) depicted in Fig. 4A. Mean ± SEM from three independent experiments is shown.

phosphatidylserine (DOPS), which are major constituents of biological membranes (32). In the presence of these lipids, CPXV012$^{36–69}$ adopted a typical α-helical CD spectrum (Fig. 5A), demonstrating that CPXV012$^{36–69}$ interacts with lipid membranes. This interaction supports the membrane binding and subsequent acquisition of an α-helical secondary structure by the ER-luminal domain of CPXV012.

To gain further insight into the behavior of CPXV012$^{36–69}$ in a membranous environment, the surface pressure of Langmuir lipid monolayers was measured in the presence of CPXV012$^{36–69}$ (Fig. 5B). As for the CD experiments, the monolayers consisted of DOPC and DOPS in a ratio of 7:3 and were formed in an aqueous buffer. The lipid monolayer surface pressure was measured by the Wilhelmy method for ~30 min after injecting CPXV012$^{36–69}$ into the monolayer subphase. A shift in the surface pressure was interpreted as penetration of the peptide into the lipid monolayer. The addition of CPXV012$^{36–69}$ to the monolayer subphase resulted in a rapid and strong increase in surface pressure, even at a biologically relevant initial surface pressure of 35 mN/m (33) (Fig. 5B). These results show that the ER-luminal domain of CPXV012 penetrates lipid monolayers and is in line with the effects observed with the CD spectra.

To investigate whether membrane penetration of CPXV012$^{36–69}$ correlates with TAP inhibition, peptides were synthesized that correspond to the alanine substitution variants depicted in Fig. 4A. The surface pressure was measured after the addition of these CPXV012-peptides to the monolayer subphase (Fig. 5C). Most variants inserted with high affinity into the DOPC/DOPS monolayer, to levels observed for wild-type CPXV012$^{36–69}$. An exception was CPXV012$^{36–69}$-Ala3, which had the lowest insertion capacity of all variants. Intriguingly, CPXV012-Ala3 also was not able to reduce MHC I surface levels, although it still interacted with the PLC (Fig. 4). This suggests that membrane insertion of the ER-luminal part of CPXV012 may be necessary for TAP inhibition. In line with this, the peptides corresponding to CPXV012-Ala1 and CPXV012-Ala7, which are capable of TAP binding and inhibition, induced a high shift in surface pressure, showing a lipid insertion comparable to the wild-type peptide.

In conclusion, the ER-luminal domain of CPXV012 variants that are capable of inhibiting TAP strongly interact with phospholipid membranes. Conversely, a CPXV012 variant that fails to inhibit TAP, but still binds to the PLC, interacts poorly with phospholipid membranes. These findings suggest that interaction with phospholipid membranes is required for TAP inhibition by CPXV012.

Discussion

CPXV dedicates two proteins to evasion of MHC class I–mediated Ag presentation. CPXV203 binds to MHC I and retains these molecules in the ER through a KDEL-like KTEL retention motif present at the C terminus of the viral protein. CPXV012 blocks MHC I peptide loading by interfering with TAP-mediated peptide transport into the ER. We studied the molecular mechanisms of TAP inhibition by CPXV012. We show that CPXV012 binds to the PLC but does not alter the overall integrity of this complex. MHC I are enriched within the PLC, which is likely caused by deficient peptide loading of MHC I that prolongs its interaction with the PLC (34). A similar effect was observed for several other viral TAP inhibitors, including BNLF2a of EBV (35), ICP47 of HSV (36), and UL49.5 of BHV (37).

Our results indicate that CPXV012 inhibits peptide transport by interfering with ATP binding to the NBDs of the TAP complex; peptide binding to TAP is unaffected. Our finding that the ER-luminal domain of CPXV012 is essential for TAP inhibition is in agreement with the previous observations that TAP is not inhibited by the larger CPXV012 homolog D10L of CPXV strains GRI-90 and GER 91-3 (17). The N-terminal 46 aa residues of these D10L proteins have a high level of amino acid sequence homology with the corresponding cytosolic and TM region of CPXV012 (Fig. 6A).

In contrast, the ER-luminal/extracellular domains of the D10L proteins show no homology with the active, ER-luminal domain of CPXV012 (17). The ER-luminal regions of these D10L proteins are extended (Fig. 6A) and make up a C-type lectin-like domain, which is suggested to be a ligand for the NK cell inhibitory receptor NKR-P1 (17). Recently, genome sequences of a number of CPXV strains from clinical isolates have been determined (38). By comparing CPXV012 homologs of these strains and of other published CPXV and orthopoxvirus strains, we identified two major clusters (Fig. 6B). Cluster 1 covers strains encoding the larger CPXV012 homologs with an extended ER-luminal domain encoding a C-type lectin-like domain, including D10L of GRI-90 and GER 91-3 (D10L-like proteins in Fig. 6B); cluster 2 contains strains encoding homologs with a truncated ER-luminal domain, similar to that of CPXV012 (CPXV012-like proteins in Fig. 6B).

A comparison of 41 genes conserved among all known poxviruses revealed that CPXV strains group into three distinct clades (38). Members of these clades are more closely related to variola virus, camelpox virus, and taterapox virus (clade 1), CPXV (clade 2), or vaccinia virus (clade 3) (38). All strains in clade 1 and the majority of the strains in clade 2 encode the truncated CPXV012-like protein, with the exception of the isolates CPXV GER-91 and CPXV HumLue09/1 (Fig. 6B). The D10L-like homologs encoded by the latter two strains are even further extended in the ER-luminal/extracellular domain compared with the other D10L-like homologs, suggesting a distinct evolutionary path for these two proteins. Other strains encoding D10L-like homologs include all CPXV strains of the vaccinia virus–like clade 3 (Fig. 6B). Furthermore, the distantly related ectromelia virus strain Moscow also encodes a D10L-like homolog. The presence of this homolog in two highly divergent orthopoxvirus species suggests that the CPXV012-like variant appeared later in virus evolution. In line with this, 16 of the 18 most recently isolated CPXV strains encode the CPXV012-like protein, supporting our hypothesis that this homolog has a more recent origin and perhaps is under greater selective pressure than are the D10L-like homologs.

Although the D10L-like variants and CPXV012-like variants lack homology within the ER-luminal domain at the amino acid level (Fig. 6A), alignment of the nucleotide sequence reveals that the genomic regions encoding these variants are highly similar at the nucleotide level (Fig. 6A). Probably, a deletion of 5 nt (underlined in Fig. 6A) within the ER-luminal domain of the larger C-type lectin-like domain-containing D10L homologs resulted in a frameshift leading to translation of the truncated ER-luminal domain present in CPXV012 and its homologs.

The ER-luminal domain of CPXV012 adopts an α-helical structure only in the presence of lipid vesicles. Indeed, prediction of the secondary structure of CPXV012 via I-TASSER suggests the existence of two helices: an N-terminal TM helix and a C-terminal α-helix (Fig. 7A). Experimental data indicate that the active domains of TAP inhibitors US6 and ICP47 also contain an α-helical secondary structure (39–41). Active US6 adopts a complex structure with 20% α-helices, whereas US6 lacking an α-helical structure is inactive (41). Structural data on the cytosolic TAP inhibitor ICP47 revealed that the active domain has no defined secondary structure in an aqueous buffer. However, like CPXV012, this domain adopts an α-helical structure in a lipid environment (40). This structural rearrangement results in high-affinity binding of ICP47 to TAP at the cytosolic interface of the ER membrane and is required for efficient TAP inhibition (39, 40).

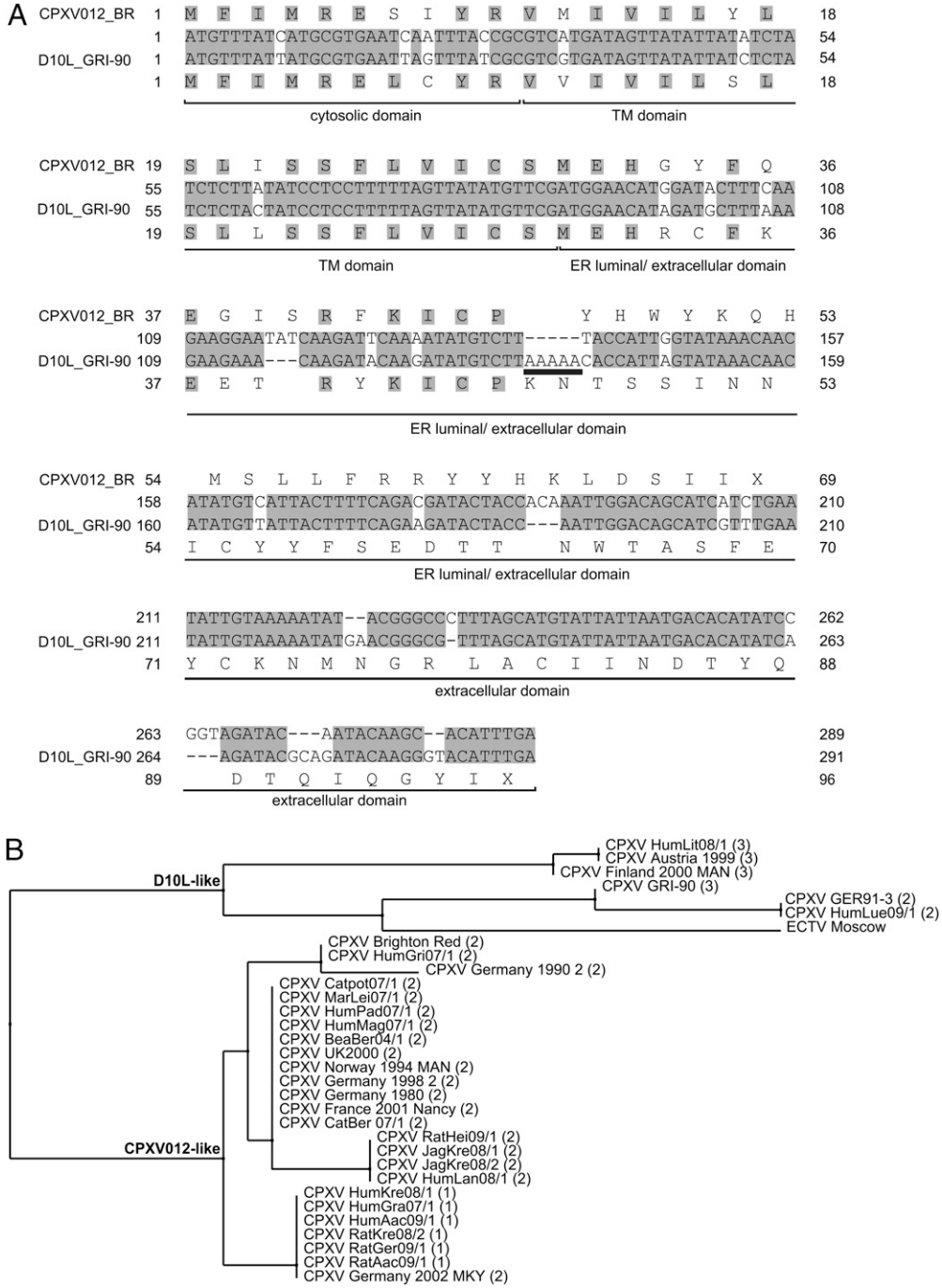

FIGURE 6. Evolutionary relationship between CPXV012 homologs. (**A**) Nucleotide and amino acid sequence alignment of CPXV012 of CPXV strain Brighton Red (BR) and D10L of CPXV strain GRI-90. Nucleotides and amino acid residues highlighted in gray are identical between the two homologs. "X" in the amino acid sequence indicates a stop codon. The underlined stretch of nucleotides indicates the position of the 5-nt deletion resulting in a frameshift, thereby encoding the truncated CPXV012 proteins. (**B**) Phylogenetic neighbor joining tree of CPXV012 homologs. Based on the percentage of identity between amino acid sequences, two groups were identified. Group 1 comprises the longer D10L-like proteins containing a C-type lectin-like domain, whereas group 2 contains proteins with a truncated ER-luminal domain, including CPXV012. Recently, three CPXV clades were identified based on phylogenetic analysis of 41 genes conserved in poxvirus (38). Clade 1 is closely related to variola virus, camelpox, and taterapox virus; clade 2 is a CPXV-like clade; and clade 3 is a vaccinia virus–like clade. The clade number is shown in parentheses for each CPXV strain. The tree was composed using Jalview from the Barton Group (University of Dundee, Scotland, U.K.) (54).

The impact of a lipid environment on the secondary structure of CPXV012$^{36–69}$ suggests that the ER-luminal domain of CPXV012 interacts with phospholipids prominently present in the ER membrane (32). This interaction was examined further using Langmuir lipid monolayers, which have been used extensively to study lipid–protein interactions (42). The extent of insertion of proteins into Langmuir lipid monolayers is proportional to the increase in surface pressure after addition of the protein to the lipid subphase. The addition of CPXV012$^{36–69}$ to the lipid subphase induced a large shift in surface pressure, thus confirming the interaction between CPXV012$^{36–69}$ and lipids.

The influence of amino acid composition of the ER-luminal domain of CPXV012 on insertion into lipid membranes was in-

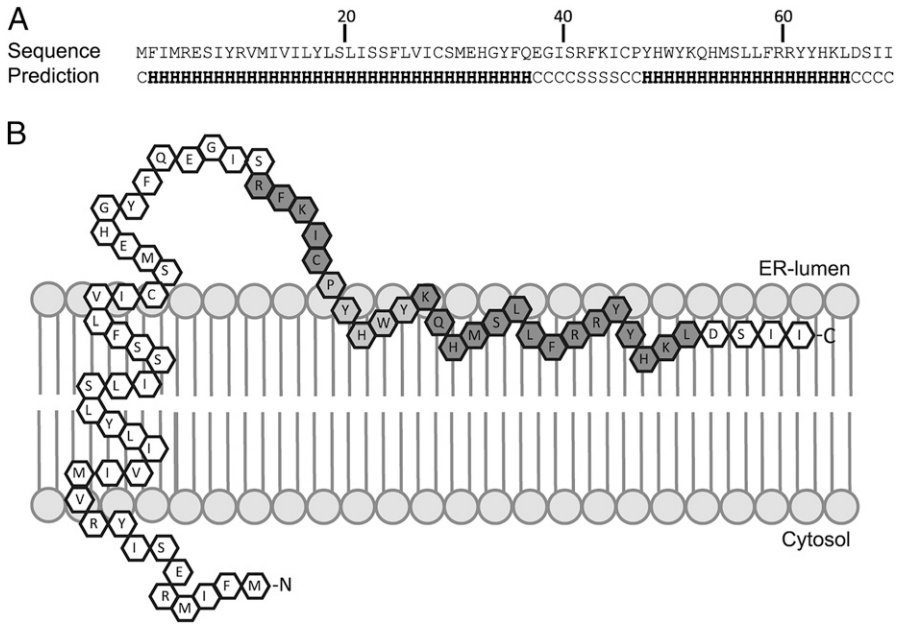

FIGURE 7. (**A**) Amino acid sequence of CPXV012 and the secondary structure predicted by the I-TASSER server (55). (**B**) Model of CPXV012 inserted into the ER membrane. Amino acid residues are depicted as hexagons. White amino acid residues are not essential for TAP inhibition. Dark gray stretches of amino acid residues are essential for TAP binding and TAP inhibition. The stretch of light gray amino acid residues is essential for TAP inhibition. C, coil; H, α-helix; S, bend.

vestigated in more detail by substituting stretches of 5-aa residues for alanines. Most substitutions within CPXV012$^{36–69}$ showed no difference in the ability to insert into the lipid monolayer, whereas the CPXV012$^{36-69}$-Ala3 mutant inserted poorly into the lipid membrane. The decreased capacity of this variant to insert into lipid monolayers may be explained by the substitution of tryptophan and tyrosine residues. Tryptophan, in particular, has a strong preference for the interfacial lipid–water region of membranes (43). Therefore, substitution of tryptophan may severely affect the insertion capacity of TM peptides. In many TM domains, including the active domain of the TAP inhibitor ICP47, tryptophan residues are located at the interfacial region, where they serve as a membrane anchor (40, 44–47).

Insertion of the active domain of CPXV012 into the ER membrane may not be crucial for interaction with TAP, because CPXV012$^{36–69}$-Ala3 inserts poorly into the monolayer, whereas the corresponding CPXV012-Ala3 protein is still able to bind to TAP. However, because CPXV012-Ala3 does not inhibit TAP transport, lipid insertion and proper anchoring into the lipid–water interface seem to be important for TAP inhibition.

The interaction between the active domain of CPXV012 and the lipid environment is remarkable, because this domain contains a number of cationic residues that are not likely to penetrate into the hydrophobic core of the ER membrane. Therefore, it is more likely that the active domain of CPXV012 resides at the lipid–water interface of the membrane (Fig. 7B). This would resemble the interaction of antimicrobial peptides with phospholipid membranes. Like CPXV012$^{36–69}$, these peptides are also cationic and form α-helical structures in the presence of lipid membranes (48). These peptides may "snorkel" parallel to the lipid–water interface, with their cationic residues extending toward the more hydrophilic part of the membrane interface (43). The pronounced affinity for a lipid environment suggests that CPXV012 has direct access to the TM domains of TAP. The 10 TM domains of TAP1 and 9 TM of TAP2 are intertwined and form a channel through the ER membrane that facilitates peptide transport. As for other ABC transporters, transport through the TM domains depends on structural rearrangements of the TM helices (22, 30). During the peptide-transport cycle, the TM helices form several conformational intermediates that depend on substrate and ATP binding to cytosolic domains of TAP (22, 49). The communication between the TM helices and the cytosolic domains is bidirectional, because the TM helices can also influence substrate and ATP binding at the cytosolic domains (50, 51). By binding directly to the TM domains of TAP, CPXV012 may lock TAP in an intermediate conformation, thereby preventing ATP binding to the cytosolic NBDs and interrupting the peptide-transport cycle. The human CMV–encoded TAP inhibitor US6, the UL49.5 proteins of EHV-1 and EHV-2, and EBV BNLF2a use a similar strategy as CPXV012, and also block ATP binding to TAP by locking TAP in an intermediate conformation (13). In contrast to CPXV012, US6 does not interact directly with the TM helices of TAP, but it binds to ER-luminal loops of TAP (52). UL49.5 also impedes conformational transitions of TAP, but its mode of interaction with its target is unknown (15). BNLF2a interferes with ATP binding through interaction with cytosolic domains of TAP (53). Apparently, structurally unrelated viral TAP inhibitors interfere with ATP binding by targeting TAP at different sites. Thus, TAP seems to be an Achilles' heel of the MHC I Ag-presentation pathway.

In conclusion, we propose the following mechanism of viral TAP inhibition. The active domain of CPXV012 mediates the interaction with TAP and is crucial for TAP inhibition. The cytosolic and TM domain of CPXV012 improves the efficiency of the active domain, possibly by stabilizing this domain and/or localizing it to the ER membrane. The ER membrane supports the formation of a secondary structure within the active domain of CPXV012. Our combined findings suggest that this domain interacts with TM helices of TAP at the interfacial region of the ER membrane. By interacting with the PLC, CPXV012 may arrest TAP in a conformational state that allows peptide binding but not the subsequent ATP-dependent peptide translocation, thus effectively preventing Ag presentation by MHC I.

Acknowledgments

We thank Gerrit Spierenburg and Koos Gaiser from the Laboratory of Translational Immunology (University Medical Center Utrecht) for technical assistance with cell sorting. We are grateful to members of the Wiertz Laboratory for helpful discussions.

Disclosures

The authors have no financial conflicts of interest.

References

1. Yewdell, J. W., E. Reits, and J. Neefjes. 2003. Making sense of mass destruction: quantitating MHC class I antigen presentation. *Nat. Rev. Immunol.* 3: 952–961.
2. Vos, J. C., P. Spee, F. Momburg, and J. Neefjes. 1999. Membrane topology and dimerization of the two subunits of the transporter associated with antigen processing reveal a three-domain structure. *J. Immunol.* 163: 6679–6685.
3. Vos, J. C., E. A. Reits, E. Wojcik-Jacobs, and J. Neefjes. 2000. Head-head/tail-tail relative orientation of the pore-forming domains of the heterodimeric ABC transporter TAP. *Curr. Biol.* 10: 1–7.
4. Procko, E., and R. Gaudet. 2009. Antigen processing and presentation: TAPping into ABC transporters. *Curr. Opin. Immunol.* 21: 84–91.
5. Sadasivan, B., P. J. Lehner, B. Ortmann, T. Spies, and P. Cresswell. 1996. Roles for calreticulin and a novel glycoprotein, tapasin, in the interaction of MHC class I molecules with TAP. *Immunity* 5: 103–114.
6. Procko, E., G. Raghuraman, D. C. Wiley, M. Raghavan, and R. Gaudet. 2005. Identification of domain boundaries within the N-termini of TAP1 and TAP2 and their importance in tapasin binding and tapasin-mediated increase in peptide loading of MHC class I. *Immunol. Cell Biol.* 83: 475–482.
7. Hansen, T. H., and M. Bouvier. 2009. MHC class I antigen presentation: learning from viral evasion strategies. *Nat. Rev. Immunol.* 9: 503–513.
8. Ahn, K., T. H. Meyer, S. Uebel, P. Sempé, H. Djaballah, Y. Yang, P. A. Peterson, K. Früh, and R. Tampé. 1996. Molecular mechanism and species specificity of TAP inhibition by herpes simplex virus ICP47. *EMBO J.* 15: 3247–3255.
9. Früh, K., K. Ahn, H. Djaballah, P. Sempé, P. M. van Endert, R. Tampé, P. A. Peterson, and Y. Yang. 1995. A viral inhibitor of peptide transporters for antigen presentation. *Nature* 375: 415–418.
10. Hill, A., P. Jugovic, I. York, G. Russ, J. Bennink, J. Yewdell, H. Ploegh, and D. Johnson. 1995. Herpes simplex virus turns off the TAP to evade host immunity. *Nature* 375: 411–415.
11. Ahn, K., A. Gruhler, B. Galocha, T. R. Jones, E. J. Wiertz, H. L. Ploegh, P. A. Peterson, Y. Yang, and K. Früh. 1997. The ER-luminal domain of the HCMV glycoprotein US6 inhibits peptide translocation by TAP. *Immunity* 6: 613–621.
12. Hengel, H., J. O. Koopmann, T. Flohr, W. Muranyi, E. Goulmy, G. J. Hämmerling, U. H. Koszinowski, and F. Momburg. 1997. A viral ER-resident glycoprotein inactivates the MHC-encoded peptide transporter. *Immunity* 6: 623–632.
13. Hewitt, E. W., S. S. Gupta, and P. J. Lehner. 2001. The human cytomegalovirus gene product US6 inhibits ATP binding by TAP. *EMBO J.* 20: 387–396.
14. Koppers-Lalic, D., E. A. Reits, M. E. Ressing, A. D. Lipinska, R. Abele, J. Koch, M. Marcondes Rezende, P. Admiraal, D. van Leeuwen, K. Bienkowska-Szewczyk, et al. 2005. Varicelloviruses avoid T cell recognition by UL49.5-mediated inactivation of the transporter associated with antigen processing. *Proc. Natl. Acad. Sci. USA* 102: 5144–5149.
15. Koppers-Lalic, D., M. C. Verweij, A. D. Lipińska, Y. Wang, E. Quinten, E. A. Reits, J. Koch, S. Loch, M. Marcondes Rezende, F. Daus, et al. 2008. Varicellovirus UL 49.5 proteins differentially affect the function of the transporter associated with antigen processing, TAP. *PLoS Pathog.* 4: e1000080.
16. Hislop, A. D., M. E. Ressing, D. van Leeuwen, V. A. Pudney, D. Horst, D. Koppers-Lalic, N. P. Croft, J. J. Neefjes, A. B. Rickinson, and E. J. Wiertz. 2007. A CD8+ T cell immune evasion protein specific to Epstein-Barr virus and its close relatives in Old World primates. *J. Exp. Med.* 204: 1863–1873.
17. Alzhanova, D., D. M. Edwards, E. Hammarlund, I. G. Scholz, D. Horst, M. J. Wagner, C. Upton, E. J. Wiertz, M. K. Slifka, and K. Früh. 2009. Cowpox virus inhibits the transporter associated with antigen processing to evade T cell recognition. *Cell Host Microbe* 6: 433–445.
18. Byun, M., M. C. Verweij, D. J. Pickup, E. J. Wiertz, T. H. Hansen, and W. M. Yokoyama. 2009. Two mechanistically distinct immune evasion proteins of cowpox virus combine to avoid antiviral CD8 T cells. *Cell Host Microbe* 6: 422–432.
19. Alzhanova, D., and K. Früh. 2010. Modulation of the host immune response by cowpox virus. *Microbes Infect.* 12: 900–909.
20. Byun, M., X. Wang, M. Pak, T. H. Hansen, and W. M. Yokoyama. 2007. Cowpox virus exploits the endoplasmic reticulum retention pathway to inhibit MHC class I transport to the cell surface. *Cell Host Microbe* 2: 306–315.
21. van Ham, S. M., E. P. Tjin, B. F. Lillemeier, U. Grüneberg, K. E. van Meijgaarden, L. Pastoors, D. Verwoerd, A. Tulp, B. Canas, D. Rahman, et al. 1997. HLA-DO is a negative modulator of HLA-DM-mediated MHC class II peptide loading. *Curr. Biol.* 7: 950–957.
22. Reits, E. A., J. C. Vos, M. Grommé, and J. Neefjes. 2000. The major substrates for TAP in vivo are derived from newly synthesized proteins. *Nature* 404: 774–778.
23. Heemskerk, M. H., E. Hooijberg, J. J. Ruizendaal, M. M. van der Weide, E. Kueter, A. Q. Bakker, T. N. Schumacher, and H. Spits. 1999. Enrichment of an antigen-specific T cell response by retrovirally transduced human dendritic cells. *Cell. Immunol.* 195: 10–17.
24. Norment, A. M., N. Lonberg, E. Lacy, and D. R. Littman. 1989. Alternatively spliced mRNA encodes a secreted form of human CD8 alpha. Characterization of the human CD8 alpha gene. *J. Immunol.* 142: 3312–3319.
25. Alvarez, E., N. Gironès, and R. J. Davis. 1990. Inhibition of the receptor-mediated endocytosis of diferric transferrin is associated with the covalent modification of the transferrin receptor with palmitic acid. *J. Biol. Chem.* 265: 16644–16655.
26. Hiemstra, H. S., G. Duinkerken, W. E. Benckhuijsen, R. Amons, R. R. de Vries, B. O. Roep, and J. W. Drijfhout. 1997. The identification of CD4+ T cell epitopes with dedicated synthetic peptide libraries. *Proc. Natl. Acad. Sci. USA* 94: 10313–10318.
27. Neefjes, J. J., F. Momburg, and G. J. Hämmerling. 1993. Selective and ATP-dependent translocation of peptides by the MHC-encoded transporter. *Science* 261: 769–771.
28. Spee, P., J. Subjeck, and J. Neefjes. 1999. Identification of novel peptide binding proteins in the endoplasmic reticulum: ERp72, calnexin, and grp170. *Biochemistry* 38: 10559–10566.
29. Khemtémourian, L., G. Lahoz Casarramona, D. P. Suylen, T. M. Hackeng, J. D. Meeldijk, B. de Kruijff, J. W. Höppener, and J. A. Killian. 2009. Impaired processing of human pro-islet amyloid polypeptide is not a causative factor for fibril formation or membrane damage in vitro. *Biochemistry* 48: 10918–10925.
30. Parcej, D., and R. Tampé. 2010. ABC proteins in antigen translocation and viral inhibition. *Nat. Chem. Biol.* 6: 572–580.
31. Procko, E., M. L. O'Mara, W. F. Bennett, D. P. Tieleman, and R. Gaudet. 2009. The mechanism of ABC transporters: general lessons from structural and functional studies of an antigenic peptide transporter. *FASEB J.* 23: 1287–1302.
32. van Meer, G., D. R. Voelker, and G. W. Feigenson. 2008. Membrane lipids: where they are and how they behave. *Nat. Rev. Mol. Cell Biol.* 9: 112–124.
33. Demel, R. A., W. S. Geurts van Kessel, R. F. Zwaal, B. Roelofsen, and L. L. van Deenen. 1975. Relation between various phospholipase actions on human red cell membranes and the interfacial phospholipid pressure in monolayers. *Biochim. Biophys. Acta* 406: 97–107.
34. Grandea, A. G., III, T. N. Golovina, S. E. Hamilton, V. Sriram, T. Spies, R. R. Brutkiewicz, J. T. Harty, L. C. Eisenlohr, and L. Van Kaer. 2000. Impaired assembly yet normal trafficking of MHC class I molecules in Tapasin mutant mice. *Immunity* 13: 213–222.
35. Horst, D., D. van Leeuwen, N. P. Croft, M. A. Garstka, A. D. Hislop, E. Kremmer, A. B. Rickinson, E. J. Wiertz, and M. E. Ressing. 2009. Specific targeting of the EBV lytic phase protein BNLF2a to the transporter associated with antigen processing results in impairment of HLA class I-restricted antigen presentation. *J. Immunol.* 182: 2313–2324.
36. Zernich, D., A. W. Purcell, W. A. Macdonald, L. Kjer-Nielsen, L. K. Ely, N. Laham, T. Crockford, N. A. Mifsud, M. Bharadwaj, L. Chang, et al. 2004. Natural HLA class I polymorphism controls the pathway of antigen presentation and susceptibility to viral evasion. *J. Exp. Med.* 200: 13–24.
37. Verweij, M. C., D. Koppers-Lalic, S. Loch, F. Klauschies, H. de la Salle, E. Quinten, P. J. Lehner, A. Mulder, M. R. Knittler, R. Tampé, et al. 2008. The varicellovirus UL49.5 protein blocks the transporter associated with antigen processing (TAP) by inhibiting essential conformational transitions in the 6+6 transmembrane TAP core complex. *J. Immunol.* 181: 4894–4907.
38. Dabrowski, P. W., A. Radonić, A. Kurth, and A. Nitsche. 2013. Genome-wide comparison of cowpox viruses reveals a new clade related to Variola virus. *PLoS ONE* 8: e79953.
39. Aisenbrey, C., C. Sizun, J. Koch, M. Herget, R. Abele, B. Bechinger, and R. Tampé. 2006. Structure and dynamics of membrane-associated ICP47, a viral inhibitor of the MHC I antigen-processing machinery. *J. Biol. Chem.* 281: 30365–30372.
40. Beinert, D., L. Neumann, S. Uebel, and R. Tampé. 1997. Structure of the viral TAP-inhibitor ICP47 induced by membrane association. *Biochemistry* 36: 4694–4700.
41. Kyritsis, C., S. Gorbulev, S. Hutschenreiter, K. Pawlitschko, R. Abele, and R. Tampé. 2001. Molecular mechanism and structural aspects of transporter associated with antigen processing inhibition by the cytomegalovirus protein US6. *J. Biol. Chem.* 276: 48031–48039.
42. Calvez, P., S. Bussières, Eric Demers, and C. Salesse. 2009. Parameters modulating the maximum insertion pressure of proteins and peptides in lipid monolayers. *Biochimie* 91: 718–733.
43. Killian, J. A., and G. von Heijne. 2000. How proteins adapt to a membrane-water interface. *Trends Biochem. Sci.* 25: 429–434.
44. Abel, E., S. L. De Wall, W. B. Edwards, S. Lalitha, D. F. Covey, and G. W. Gokel. 2000. Formation of stable vesicles from N- or 3-alkylindoles: possible evidence for tryptophan as a membrane anchor in proteins. *J. Org. Chem.* 65: 5901–5909.
45. Strandberg, E., and J. A. Killian. 2003. Snorkeling of lysine side chains in transmembrane helices: how easy can it get? *FEBS Lett.* 544: 69–73.
46. Yau, W. M., W. C. Wimley, K. Gawrisch, and S. H. White. 1998. The preference of tryptophan for membrane interfaces. *Biochemistry* 37: 14713–14718.
47. Neumann, L., W. Kraas, S. Uebel, G. Jung, and R. Tampé. 1997. The active domain of the herpes simplex virus protein ICP47: a potent inhibitor of the transporter associated with antigen processing. *J. Mol. Biol.* 272: 484–492.
48. Eiríksdóttir, E., K. Konate, U. Langel, G. Divita, and S. Deshayes. 2010. Secondary structure of cell-penetrating peptides controls membrane interaction and insertion. *Biochim. Biophys. Acta* 1798: 1119–1128.
49. Geng, J., S. Sivaramakrishnan, and M. Raghavan. 2013. Analyses of conformational states of the transporter associated with antigen processing (TAP) protein in a native cellular membrane environment. *J. Biol. Chem.* 288: 37039–37047.

50. Crowley, E., M. L. O'Mara, I. D. Kerr, and R. Callaghan. 2010. Transmembrane helix 12 plays a pivotal role in coupling energy provision and drug binding in ABCB1. *FEBS J.* 277: 3974–3985.
51. Kueppers, P., R. P. Gupta, J. Stindt, S. H. Smits, and L. Schmitt. 2013. Functional impact of a single mutation within the transmembrane domain of the multidrug ABC transporter Pdr5. *Biochemistry* 52: 2184–2195.
52. Halenius, A., F. Momburg, H. Reinhard, D. Bauer, M. Lobigs, and H. Hengel. 2006. Physical and functional interactions of the cytomegalovirus US6 glycoprotein with the transporter associated with antigen processing. *J. Biol. Chem.* 281: 5383–5390.
53. Horst, D., V. Favaloro, F. Vilardi, H. C. van Leeuwen, M. A. Garstka, A. D. Hislop, C. Rabu, E. Kremmer, A. B. Rickinson, S. High, et al. 2011. EBV protein BNLF2a exploits host tail-anchored protein integration machinery to inhibit TAP. *J. Immunol.* 186: 3594–3605.
54. Waterhouse, A. M., J. B. Procter, D. M. Martin, M. Clamp, and G. J. Barton. 2009. Jalview Version 2—a multiple sequence alignment editor and analysis workbench. *Bioinformatics* 25: 1189–1191.
55. Zhang, Y. 2008. I-TASSER server for protein 3D structure prediction. *BMC Bioinformatics* 9: 40.